Science of the Total Environment 639 (2018) 374–384

Contents lists available at ScienceDirect

Science of the Total Environment

journal homepage: www.elsevier.com/locate/scitotenv

# Shifts in wind energy potential following land-use driven vegetation dynamics in complex terrain

Jiannong Fang[a], Alexander Peringer[b], Mihai-Sorin Stupariu[c,d], Ileana Pătru-Stupariu[d,e], Alexandre Buttler[f,g,h], Francois Golay[i], Fernando Porté-Agel[a,*]

[a] Wind Engineering and Renewable Energy Laboratory (WiRE), School of Architecture, Civil and Environmental Engineering (ENAC), École Polytechnique Fédérale de Lausanne (EPFL), Lausanne 1015, Switzerland
[b] Landscape Ecology and Resources Management, Faculty FLUS-HKT, Nuertingen-Geislingen University, Germany
[c] Faculty of Mathematics and Computer Science, University of Bucharest, Romania
[d] Transdisciplinary Research Centre Landscape-Territory-Information Systems (CeLTIS), Institute of Research of University of Bucharest (ICUB), Romania
[e] Department of Regional Geography and Environment, Faculty of Geography, University of Bucharest, Romania
[f] Ecological Systems Laboratory (ECOS), School of Architecture, Civil and Environmental Engineering (ENAC), École Polytechnique Fédérale de Lausanne (EPFL), Lausanne 1015, Switzerland
[g] Swiss Federal Institute for Forest, Snow and Landscape Research (WSL), Site Lausanne, Station 2, Lausanne 1015, Switzerland
[h] Laboratoire de Chrono-Environnement, UMR CNRS 6249, UFR des Sciences et Techniques, Université de Franche-Comté, 16 route de Gray, F-25030 Besançon, France
[i] Geographic Information Systems Laboratory (LASIG), School of Architecture, Civil and Environmental Engineering (ENAC), École Polytechnique Fédérale de Lausanne (EPFL), Lausanne 1015, Switzerland

## HIGHLIGHTS

- Modeling framework coupling large-eddy simulation of boundary layer, vegetation dynamics and digital elevation model.
- Wind energy potential in complex mountain terrain strongly depends on land cover changes driven by land-use change.
- Trade-off between renewable energy production and biodiversity under agro- and forest policies in landscape development.
- The framework could support the long-term planning of wind energy projects under land-use and climate change scenarios.

## GRAPHICAL ABSTRACT

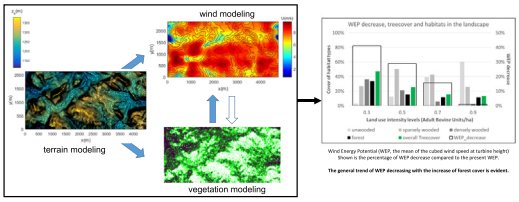


## ARTICLE INFO

*Article history:*
Received 30 November 2017
Received in revised form 30 April 2018
Accepted 6 May 2018
Available online 26 May 2018

Editor: R. Ludwig

## ABSTRACT

Many mountainous regions with high wind energy potential are characterized by multi-scale variabilities of vegetation in both spatial and time dimensions, which strongly affect the spatial distribution of wind resource and its time evolution. To this end, we developed a coupled interdisciplinary modeling framework capable of assessing the shifts in wind energy potential following land-use driven vegetation dynamics in complex mountain terrain. It was applied to a case study area in the Romanian Carpathians. The results show that the overall shifts in wind energy potential following the changes of vegetation pattern due to different land-use policies can be dramatic. This suggests that the planning of wind energy project should be

* Corresponding author.
*E-mail address:* fernando.porte-agel@epfl.ch (F. Porté-Agel).

https://doi.org/10.1016/j.scitotenv.2018.05.083
0048-9697/

*Keywords:*
Atmospheric boundary layer
Model coupling
Large-eddy simulation
Digital elevation model
Wood-pasture model
Land cover

integrated with the land-use planning at a specific site to ensure that the expected energy production of the planned wind farm can be reached over its entire lifetime. Moreover, the changes in the spatial distribution of wind and turbulence under different scenarios of land-use are complex, and they must be taken into account in the micro-siting of wind turbines to maximize wind energy production and minimize fatigue loads (and associated maintenance costs). The proposed new modeling framework offers, for the first time, a powerful tool for assessing long-term variability in local wind energy potential that emerges from land-use change driven vegetation dynamics over complex terrain. Following a previously unexplored pathway of cause-effect relationships, it demonstrates a new linkage of agro- and forest policies in landscape development with an ultimate trade-off between renewable energy production and biodiversity targets. Moreover, it can be extended to study the potential effects of micro-climatic changes associated with wind farms on vegetation development (growth and patterning), which could in turn have a long-term feedback effect on wind resource distribution in mountainous regions.

© 2018 Elsevier B.V. All rights reserved.

## 1. Introduction

As a safe and renewable non-polluting resource, wind energy has been undergoing a large-scale development worldwide in the past decade. With the continuous advance of wind power technology and decrease of its effective costs, it is foreseen that wind power penetration levels will continue to increase in many countries. Accurate wind energy potential assessments are crucial to the successful development of wind power plants. Knowing the spatial distribution of wind and turbulence at a specific site guides the wind power planners to select the wind farm site, evaluate the production and cost, and optimize the micro-siting of wind turbines to maximize wind energy production and minimize fatigue loads.

There are two main methods for assessing wind energy potential: one is based on observational data and the other relies on numerical wind field simulations. In practice, the two methods are often combined to produce wind resource maps which, in some countries/regions such as Canada, USA, and Europe, are collected together as national wind atlases. Various wind flow modeling systems targeted at different scales have been developed and applied to wind resource assessment. Examples of mesoscale systems include the widely used Weather Research and Forecasting (WRF) model (Skamarock et al., 2008) developed for both research and operational purposes and the operational Consortium for Small-scale Modeling (COSMO) model (Nolan et al., 2014). Mesoscale modeling typically covers a domain size of $10^7$ m to $10^5$ m with a grid resolution of $10^5$ m to $10^3$ m. Generally, several levels of physical downscaling by domain nesting are required within these ranges to overcome the computational complexity. Initial and boundary conditions are obtained from large scale weather models like the Global Forecast System (GFS) produced by the National Centers for Environmental Prediction (NCEP). Many studies have validated mesoscale models such as WRF and apply them for wind resource assessment and wind power forecast. So far satisfactory results have been reported mainly for cases where the terrain features are simple. For example, Hahmann et al. (2015) show that WRF is able to predict the annual mean wind speed within the measurement uncertainty in the North and Baltic Seas. It is worth mentioning that global wind data, based on WRF is now available (https://www.globalwindatlas.info/). However, in complex terrain, mesoscale models tend to yield considerable errors for both wind speed and wind direction predictions (Jiménez and Dudhia, 2012, 2013). This is mainly due to the fact that effects of local topography and land cover are insufficiently captured at relatively coarse grid resolutions in mesoscale models. To tackle this problem, further downscaling to microscale is required. Recently, the coupling of mesoscale and microscale models has become a strong area of research for the next generation of wind resource assessment. This is because it can better handle the multi-scale nature of the problem by simulating the various physical processes directly and capture both large scale weather and microscale topography effects on local wind conditions (Moeng et al., 2007; Carvalho et al., 2013; Gopalan et al., 2014; Castro et al., 2015; Bilal et al., 2016; Sanz Rodrigo et al., 2017).

A microscale model typically adopts a domain size ranging from 1 to 20 km and a grid resolution ranging from 1 to 100 m. The majority of microscale models apply Computational Fluid Dynamics (CFD) techniques to solve the Navier-Stokes (N-S) equations governing turbulent flows in the atmospheric boundary layer (ABL) with stationary forcing (i.e. mesoscale tendencies are neglected). Among the various CFD methods, Large-Eddy Simulation (LES) based on the spatially-filtered N-S equations has become an important tool for simulating turbulent flows. LES has been successfully validated and applied for the study of ABL flows over homogeneous terrain. The development and application of LES-based numerical models for wind field simulations over complex terrain is on the rise (Wan et al., 2007; Silva Lopes et al., 2007; Wood, 2000; Wan and Porté-Agel, 2011; Diebold et al., 2013; Bechmann and Sørensen, 2011; Cheng and Porté-Agel, 2013; Mirocha et al., 2014; Liu et al., 2016; Fang and Porté-Agel, 2016; Shamsoddin and Porté-Agel, 2017). To apply LES to complex heterogeneous terrain, however, there is a need for coupling it with high-resolution data of the relevant surface properties, namely surface elevation (topography) and land cover. Conventionally, Monin Obukhov Similarity Theory (MOST) is used as surface-layer scheme to relate vegetation with the turbulent fluxes in the near-wall gird cells by assigning corresponding aerodynamic surface roughnesses, while obstacles and tall canopies are explicitly modeled in CFD when they are directly influencing the sites of interest. So far, in numerical wind field simulations, vegetation was treated as a static surface property like topography and little research has been done to study the long-term impacts of vegetation dynamics on local wind conditions and their implications on wind energy project planning.

The need to address landscape structural dynamics can be derived from the 2009 European Environment Agency Report concerning Europe's onshore and offshore wind potential. Among the steps to be addressed in the future, the report explicitly mentions the necessity of a more detailed analysis of areas where model prediction and observed wind velocities differed most, notably mountainous and forested areas. Furthermore, the analysis of specific vulnerabilities of biodiversity related to specific bird and other species and of landscapes was requested, as well as the explicit consideration of such vulnerabilities in mapping wind energy potential in Europe.

In mountainous regions, a high potential for wind turbines exists, especially at higher altitudes and on the crests of these middle-range mountains. For example, the Juvent wind farm in the Jura mountains of Switzerland has 16 wind turbines installed on two hills, Mont Soleil (alt. 1291 m) and Mont Crosin (alt. 1268 m), where the land cover varies from grasslands to forests. Unfortunately, these regions are also often very sensitive to turbine installations, because of their high value in terms of biodiversity and landscape scenery (Bergmeier et al., 2010; Etienne, 1996). During the past decades, at higher altitudes there was a drastic land-use and landcover change,

driven by change in agro-policy. More emphasis was put on productive lowlands and subsidies for low-intensity land-use forms in the mountains decreased (Perrenoud et al., 2003). This resulted in the reduction of land-use intensity, if not abandonment, and led to forest encroachment on former mountain pastures. Historical photographs show that thickets established on large pasture areas within 30 years (Barbezat and Boquet, 2008; Dovčiak et al., 2008).

We address the Southern Carpathian mountains in Romania, where this conflict is dramatic because of major shifts in agro-policy and land-use practices in the post-communist period (Maruska et al., 2012). As in many European mountainous regions, wooded pastures are a traditional land use form and an important part of the cultural heritage, as in the Carpathian mountains. Moreover, pasture-woodlands are a semi-natural landscape (Buttler et al., 2009) that is especially rich in biodiversity when compared to grasslands and forests (Gillet et al., 1999; Dufour et al., 2006). Unfortunately, wooded pastures are very sensitive to land-use changes (Peringer et al., 2013). Wooded pastures cover large areas, predominantly at higher elevations, where herding of livestock cleared the landscape in the past and contributed to the today's high wind potential. Land abandonment following agro-political changes is followed by patch-wise forest development on former grasslands. In a meta-analysis conducted at the level of the whole Carpathian region (Munteanu et al., 2014) it was mentioned that, during communism and in the post-communist period, in Romania forest loss and land abandonment were parallel processes induced by different drivers: economic, political and socio-demographic. A regional study (Pătru-Stupariu et al., 2016) conducted in surroundings of the Fundata site showed that indeed, between 1912 and 1980, the forest cover reduced its surface almost by half while the pastures almost doubled their surface. Conversely, the time period 1980–2009 is characterized by a slight forest regrowth, of almost 10%, to the detriment of pastures. This process is highly likely to continue and even become more widespread in the future, and can be expected to influence wind energy potential by an increase of surface roughness and is known to threaten landscape-scale biodiversity.

The modeling of vegetation dynamics in wooded pastures as a response to various scenarios of land-uses requires a process-based approach that incorporates the major ecological processes of tree recruitment and growth, and the influence of livestock while grazing and browsing (Gillet, 2008). A high spatial resolution is required to mimic the establishment of young trees close to their seed parents and thereby the realistic formation of a woodland-grassland mosaic that implies a high surface roughness and major effects on wind flow (Peringer and Rosenthal, 2011). Moreover, a balanced representation of the ecology of woody plants, grassland communities and livestock is required to ensure a reliable model response to scenario parameters and across large areas with complex topography and variable growth conditions for trees and forage for livestock (Weisberg et al., 2006). In general, appropriate models of pasture-woodland dynamics are few, but the wood-pasture model WoodPaM (Gillet, 2008) was applied in the Southern Carpathians recently and demonstrated reasonable landscape structural changes according to distinct land-use intensities and agro-political recommendations (Peringer et al., 2016).

Based on these recent advances in wind resource assessment, vegetation dynamics and terrain modeling, we aim to develop a modeling framework capable of assessing the shifts in wind energy potential following vegetation dynamics in mountain landscapes and apply it to a case study to obtain relevant guidelines for the long-term planning of wind energy projects over complex terrain. To achieve this, we developed an interdisciplinary approach that consists of coupling three building blocks: wind modeling, terrain modeling, and vegetation modeling. The wind modeling block is based on a new-generation tuning-free LES technique for high-resolution eddy-resolving simulations of wind and turbulence over complex terrain. The terrain modeling block consists of very high resolution Digital Elevation Models (DEMs) linked with suitable, wavelet-based generalization and filtering techniques to provide description of the land surface properties at the relevant scales. The vegetation modeling block adopts the dynamic landscape and vegetation model (WoodPaM) to develop a set of alternative tree cover mosaics for a range of land-use intensities in the Southern Carpathian pasture-woodlands. Through the use of a terrain-following coordinate transformation and similarity-theory-based wall modeling, LES is coupled with high-resolution information of the relevant land surface properties obtained from the terrain and vegetation modeling blocks. The proposed modeling framework is applied to a case study area in the Romanian Carpathians for which high resolution terrain data are available. The driving questions are as follows: (1) To what extent does the wind energy potential in mountain landscapes depend on complex topography and vegetation structure? (2) Do the vegetation dynamics and shifts in vegetation structure caused by land-use change impact the wind energy potential? (3) What are the subsequent implications on wind power planning?

## 2. Modeling framework

### 2.1. Study site

The study area (Fig. 1) is at Fundata in the Southern Romanian Carpathians, for which high resolution geographical survey data are available, hence it allows a synergistic combination of the three above-mentioned modeling blocks. The study site has a total surface 27.46 $km^2$ and the altitude ranges between 930 m and 1400 m. The vegetation cover is a mixture of ungrazed forest and wooded pastures (Pătru-Stupariu et al., 2017). It is worth mentioning that the characteristics and patterns of Fundata are similar to those of the sites in the Swiss Jura mountains where wind energy is under fast development.

### 2.2. Wind modeling

We used a new-generation tuning-free LES framework developed at the Wind Engineering and Renewable Energy Laboratory (WiRE) of EPFL (hereafter called WiRE-LES). The details of WiRE-LES are provided in Appendix A. The WiRE-LES has been extensively validated in a variety of canonical flow conditions over both flat terrain and simple topography (Porté-Agel et al., 2000; Wan et al., 2007; Stoll and Porté-Agel, 2008; Wan and Porté-Agel, 2010; Wu and Porté-Agel, 2011; Lu and Porté-Agel, 2011; Cheng and Porté-Agel, 2013; Fang and Porté-Agel, 2016; Shamsoddin and Porté-Agel, 2017). Yet, wind field in mountainous region is highly turbulent and it is strongly modulated by local, non-linear interactions with the underlying multi-scale topography and heterogeneous vegetation cover. Furthermore, geomorphology and extensive land use in mountainous regions lead to the evolution of vegetation cover resulting in complex heterogeneous patterns, such as forest-grassland mosaics of pasture-woodlands. To apply the WiRE-LES under such complex and dynamic surface conditions, we couple it with high-resolution data of the relevant surface properties obtained from the terrain and vegetation modeling blocks described in the next two subsections. The high-resolution data of the topography is directly used as input to the WiRE-LES to determine the surface elevation $z_s$ for the generation of the computational grid. The high-resolution data of the vegetation cover is first used to calculate the canopy height ($h$) and density ($\lambda$). Then, those properties are used to determine the roughness length ($z_0$) and displacement height ($d$) in the wall model expressed by Eq. (A.4). In this study, the analytic expression proposed by Raupach (1994) is used to calculate $z_0$ and $d$ as functions of $h$ and $\lambda$.

The computational domain for the LES and WoodPaM simulations, along with the surface elevation distribution, are shown in

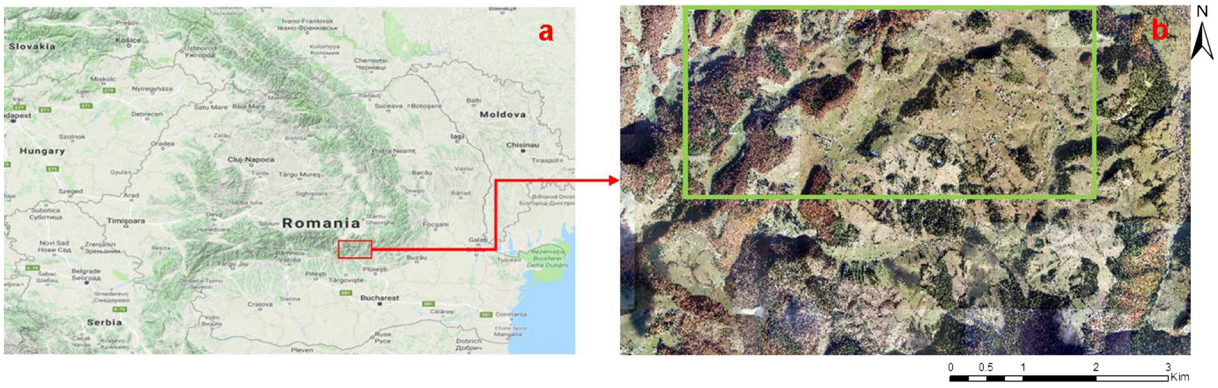


**Fig. 1.** a) Location of the study site in the Romanian Carpathians (source: Google Maps). b) Orthophotomap of the study site. The coordinates of the lower left corner are 45°24′54″ N and 25°14′23″ E. The rectangle delineated in green represents the computational domain of the wind and vegetation simulations.

Fig. 2. A neutrally stratified atmospheric boundary-layer flow over this mountainous region is simulated by the WiRE-LES for different surface vegetation patterns. The maximum slope here is below 45°, so the TFCT method (see Appendix A for details) is used to represent the topography. The boundary-layer height is set to 1000 m above the mean surface elevation. Considering the fact that the area has a characteristic strong west-wind (Dragomir et al., 2016), the flow is driven by a constant mean pressure gradient along the $x$ direction. The domain is discretized into 192 × 96 × 96 points, resulting in a grid resolution of $dx = dy = 25$ m and $dz \approx 10$ m. Periodic boundary conditions are applied in the horizontal directions. The upper boundary condition is specified as stress-free. The bottom boundary condition is no penetration together with the wall stress determined according to Eq. (A.4). For each landcover scenario, the large-eddy simulation is first run for a long enough time to guarantee that the quasi-steady conditions are reached. The LES results are then averaged in time to yield statistics for the comparison between different landcover scenarios.

To have a quantitative measure on the shift of wind energy potential and its relationship with the landscape evolution, here we introduce an indicator of wind energy potential, called WEP. It is defined as

$$\mathrm{WEP} = \left\langle U^3 \right\rangle \tag{1}$$

where $U$ is the hub-height time-averaged wind speed and $\langle\rangle$ denotes the spatial averaging performed over the places with elevations

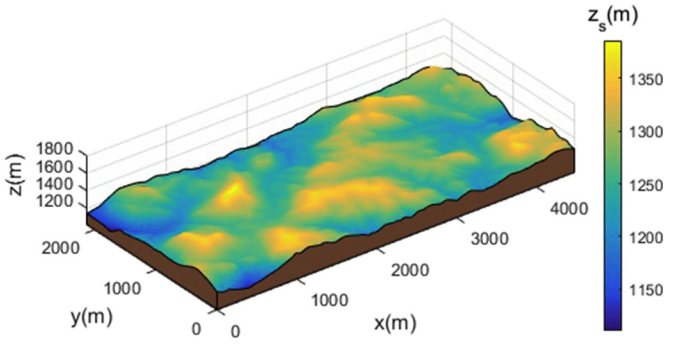


**Fig. 2.** The computational domain for the large-eddy simulation (LES) and WoodPaM simulations. Here $z$ is the elevation from sea level in m and $z_s$ is the surface elevation.

higher than the mean elevation, which are usually favorable for the installation of wind turbines.

### 2.3. Terrain modeling

The terrain modeling relied on processing a high resolution LiDAR data set. The data was collected in October 2013 by the company *Primul Meridian* through customized airborne laser scanning. The company processed and classified the points by using the TerraScan software package, as follows. In a first stage, the classification was made automatically by the internal algorithms of TerraScan. Then, in a second stage, in the cases where the algorithms did not yield the expected results, e.g. due to ground morphology, they used the TerraScan tools for performing a manual classification. Finally, the company provided the classified point cloud in the LAS-data format.

The average point density was 22.5 points per square meter, such that fine vegetation features became visible in the point cloud (Fig. 3). The points were classified by the company as ground (152,378,749 points), vegetation (461,054,334 points) and other classes - including buildings, hay stacks, other constructions such as fences (5,706,879 points). The average point spacing was 0.48 m for the ground and 1.65 m for the vegetation.

We used the ArcGIS 10.1 software for producing 1 m raster grids representing (i) the Digital Terrain Model (DTM) - derived only from the ground points, by actually taking into account the last returns of the LiDAR pulses, (ii) the Digital Surface Model (DSM) - we used the points classified as vegetation for deriving the model; (iii) the Canopy Height Model (CHM) - it was derived as raster difference between the DSM and the DTM; (iv) the Canopy Density Model (CDM) - produced from the vegetation points. For deriving the models from the point cloud, we used natural neighbor as interpolation method, with ground belonging to the DSM, because they performed better than linear interpolation and ground not included in the DSM. The comparison relied on visual checks of the output and on the computation of some basic statistics of the CHM grids: maximum, minimum, mean, standard deviation, percentage of negative canopy and percentage of canopy above 30 m, respectively (Table 1).

We performed additional corrections to the DTM, CHM and CDM before using them in the wind and vegetation models. This included removing 'no data' cells and changing cells with negative canopy values to zero. By adjusting the number of rows and columns to be divisible by 25, we finally generated, through standard averaging techniques, DTM, CHM and CDM grids with a cell size of 25 m. The grids had 147 rows and 245 columns, thus covering a surface of 22.51 km$^2$ and they were further used for the wind and vegetation modeling.

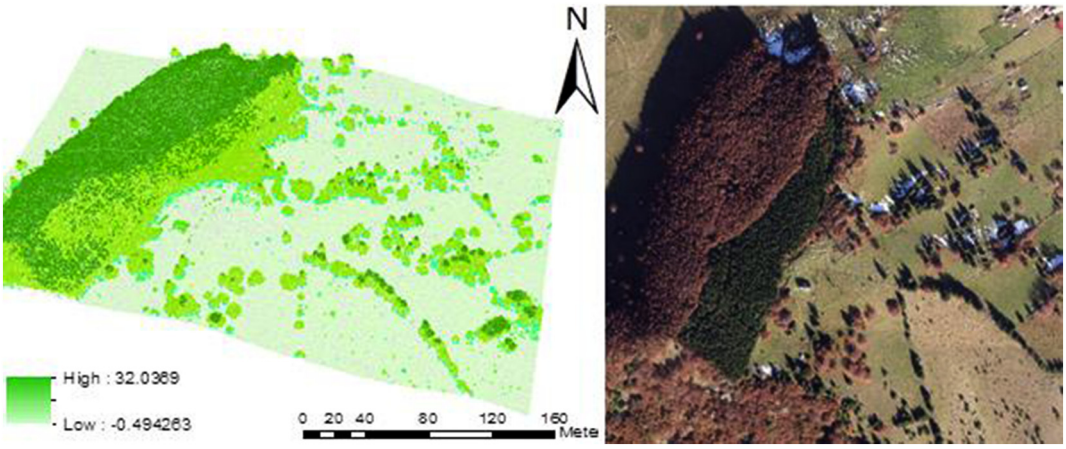


**Fig. 3.** Left: 3D view of the ground and vegetation points for a sample of the LiDAR data. The color ramp represents the height above ground. Right: aerial photo of the actual terrain. (For interpretation of the references to color in this figure legend, the reader is referred to the web version of this article.)

### 2.4. Vegetation modeling

The spatially explicit dynamic model WoodPaM (Gillet, 2008) was designed to simulate vegetation dynamics in pasture-woodlands dependent on the multiple traditional and extensive land use forms, including cattle stocking and logging. The model incorporates most of the processes necessary to predict the long-term impact of silvopastoral management and climate change on herbaceous and forest plant communities, as well as cattle habitat use in heterogeneous pasture-woodlands (Peringer et al., 2013). WoodPaM is a grid-based simulation model, with each cell being 25 m wide. It features an individual-based submodel of tree regeneration and spread, which predicts the structure of forest stands located in a grid cell and in neighboring cells. In contrast to forest landscape models, WoodPaM is able to realistically simulate gradients from open grassland to closed forest continuously in space and time. The routines for widespread tree establishment in grasslands allow modeling of the characteristic patch-mosaic of grassland and forest prevalent in the study area.

WoodPaM was applied to simulate a set of alternative forest-grassland mosaics in the study area based on scenarios of different land-use intensities. These mosaics were simulated to develop since 1650 CE (beginning of intensive land-use in the area) over a period of 350 years until 2000 CE under the assumption of constant grazing pressure (and tree cutting). The entire landscape was initially pastured except for large and dense forests shown in Figs. 4 and 5 as dense and tall stands of trees (light blue for canopy height and yellow for canopy density). These are generally dominated by beech, which indicates an exclusion from grazing by forest management, because browsing intolerant beech cannot regenerate under herbivore pressure. The differences among simulated landscapes therefore show fundamental relationships among land-use intensity and landscape structure expressed by tree cover distribution but do not show successional dynamics for land-use intensification or extensification. Although not shown directly, the consequences of future land-use change will be discussed. Any prospective simulations for the future consequences of land-use change were hindered by the lack of appropriate climate change scenarios in the area, whereas historic climate data was at hand.

The land-use scenarios were distinguished by the density of livestock, which determines grazing pressure on vegetation and economic yield for farmers. Livestock densities were set to 0.3, 0.5, 0.7 and 0.9 Adult Bovine Units (ABU) per hectare for 124 days/year. These values reflect the minimum, the optimal and the maximum livestock densities according to the Romanian management guidelines for sustainable use of pasture-woodlands (Maruska et al., 2012). The intensive grazing with 0.9 ABU/ha aimed to indicate overuse that in the long run leads to pastures with almost no trees. The low-intensity scenario with 0.3 ABU/ha aimed to indicate a landscape dominated by forest with only small grassland area. Wood exploitation was simulated as single-tree cutting and set to a return interval of the cut down of trees in a grid cell of 200 years because of slow tree growth in the mountain climate. It was the same for all grazing scenarios and thus reflects the low-intensity exploitation of forest for fire wood by the local people.

The model output at the end of simulations (year 2000 CE) was the number of tree individuals per grid cell in 4 height classes. In order to estimate the nature conservation value of the simulated landscapes, the tree cover per grid cell was estimated from the tree individuals and was classified into habitat types that harbor specific biodiversity, namely unwooded, sparsely and densely wooded pasture and forest (Gallandat et al., 1995). Transferred to the LES

**Table 1**
Basic statistics of the canopy height model (CHM) for the four possibilities to generate the model: interpolation methods - L(inear) and N(atural) N(eighbor) and ground belongs to the digital surface model (DSM) (yes/no).

| Interp. method | Ground in DSM | Max | Min | Mean | Std. dev. | Negative CHM (%) | Canopy > 30 m (%) |
|---|---|---|---|---|---|---|---|
| L | Yes | 65.18 | −2.03 | 4.48 | 7.22 | 0.44 | 0.15 |
| L | No | 141.59 | −9.31 | 4.85 | 7.49 | 0.81 | 0.17 |
| NN | Yes | 61.10 | −0.48 | 4.48 | 7.15 | 0.18 | 0.12 |
| NN | No | 98.86 | −7.68 | 4.85 | 7.45 | 0.56 | 0.15 |

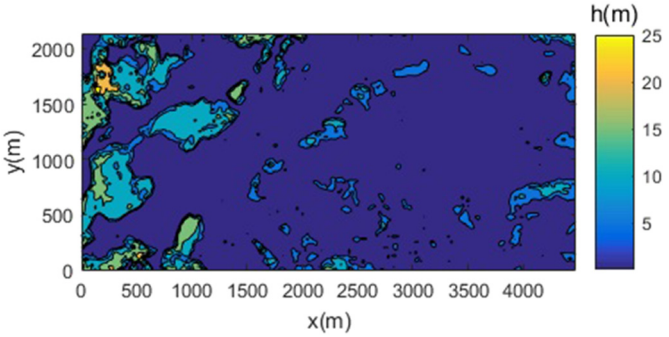


**Fig. 4.** The present canopy height at Fundata site in the Romanian Carpathians.

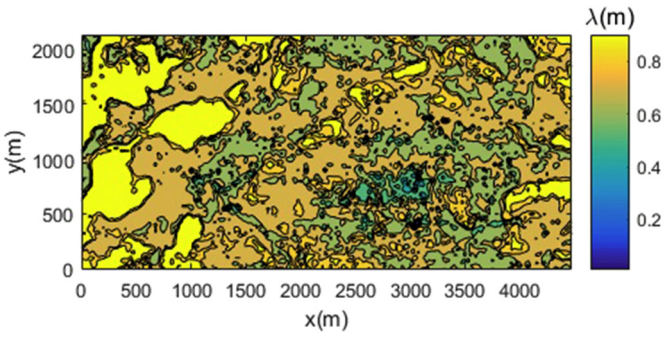


**Fig. 5.** The present canopy density at Fundata site in the Romanian Carpathians.

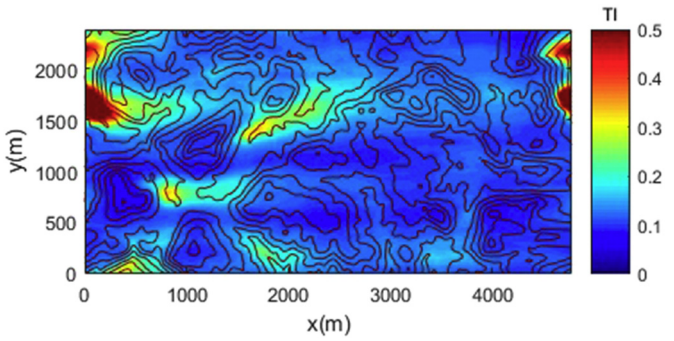


**Fig. 7.** The turbulence intensity at the turbine hub height of 100 m simulated by the WiRE-LES modelling framework for the present landscape at Fundata site in the Romanian Carpathians. Here the solid contour lines show the elevation.

wind modeling framework are the canopy height and density values per cell estimated based on the physical class of vegetation cover per cell. These values were then translated into the surface roughness and displacement height values as explained in the Section 2.2. Altogether, scenario simulations demonstrated the long-term consequences of different land-use intensities in mountain pasture-woodlands and provided information for the estimate of WEP, nature conservation value and farmer's income based on livestock densities.

## 3. Results and discussions

For the current land cover, the high-resolution maps of canopy height and density obtained by the terrain modeling are shown in Figs. 4 and 5, respectively. The mean wind speed field and turbulence intensity (TI) at the turbine hub height of 100 m predicted by the WiRE-LES for the current land cover are presented in Figs. 6 and 7, respectively. Later, this simulation case is used as a reference for the evaluation of shifts in wind energy potential following vegetation dynamics with different land-use scenarios.

Vegetation patterns in the computational domain (Fig. 2) for a series of land-use scenarios that compare agro-economic recommendations for the management of Romanian pasture-woodland landscapes (Maruska et al., 2012; Peringer et al., 2016) are shown in Fig. 8. Under intensive grazing a very open landscape with only few and scattered isolated trees emerged (Fig. 8a). The overuse of pasture woodlands led to structural simplicity. Under maximum grazing, the density of scattered trees was higher throughout the landscape. A realistic wood-pasture mosaic landscape emerged as it was predicted by the management guideline for pasture-woodland conservation. Under optimum grazing, forest patches developed predominantly on the valley slopes that are unattractive for livestock but large pastures with only scattered trees were found on the hilltops (compare Figs. 2 and 8c). This landscape pattern provides the different habitat types namely unwooded, sparsely and densely wooded pasture and forest

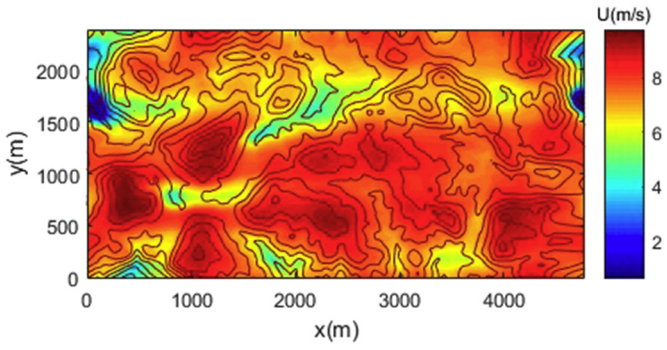


**Fig. 6.** The mean wind speed field at the turbine hub height of 100 m simulated by the WiRE-LES modelling framework for the present landscape at Fundata site in the Romanian Carpathians. Here the solid contour lines show the elevation.

in the most balanced manner (Fig. 10), which is causal for the highest ($\gamma$-)biodiversity at landscape scale and corresponds to the underlying recommendation of "optimum grazing". Grassland and forest habitats are almost equally present and satisfy the requirements for very distinct groups of target species. Forest-grassland ecotones with varying conditions (sparsely and densely wooded pastures) are the key habitat for pasture-woodlands and reach their highest cover. The other scenarios either favor grassland or forest on the cost of each other. In the minimum grazing scenario (Fig. 8d), the valleys were filled with forest, the size of open pastureland was small and even on the hilltops the scattered trees were more dense.

The intensive grazing scenario led to a landscape structure that corresponded to current conditions. This can be understood as a legacy effect from the communist period, when land-use was intensive even in remote regions. The widespread cover of low canopy in Figs. 4 and 5, however, shows that early successional shrub establishment is present following post-communist land-use extensification. In a nutshell, the scenarios demonstrate a strong and combined influence of land-use intensity and topography on the tree cover distribution.

The WiRE-LES was applied to simulate wind and turbulence over the study area for the four land-use scenarios. Fig. 9 shows the mean wind speed shifts at the surface of the turbine hub height for the scenario landscapes with respect to the current one. The results demonstrate that the wind field in complex mountain terrain strongly depends on land cover and corresponding land use. Different structure of forest-grassland mosaic patterns could affect the wind speed dramatically, thus having a significant impact on the power output from wind turbines/farms to be installed locally. Whereas the wind speed pattern for the intensive grazing scenario only slightly differs from the current state (Fig. 9a), strong deviations towards lower wind speed are shown for the scenarios with lower grazing intensity. Slowing down the wind flow already sets in with slight densification of the scattered trees on the hilltop pastures (Fig. 9b for maximum grazing). The development of a structurally rich mosaic landscape under optimum grazing broadens this effect (Fig. 9c). With minimum grazing the entire landscape is affected (Fig. 9d).

Despite the overall trend of decreasing wind speed with lowering grazing pressure, locally, the mean wind speed at the turbine hub height can either increase or decrease compared to the current situation. For example, Fig. 9a shows a maximum increase of 3.6 m/s and a maximum decrease of 1.8 m/s, respectively.

Fig. 10 shows the decrease of WEP relative to the current situation and in relation to the cover of habitat types in the four scenario landscapes. The area covered by each habitat was estimated from the maps in Fig. 8a–d and provides information on the spatial distribution of trees more detailed than tree cover does. The results show that, for high grazing pressures (high ABUs), the WEP decrease is

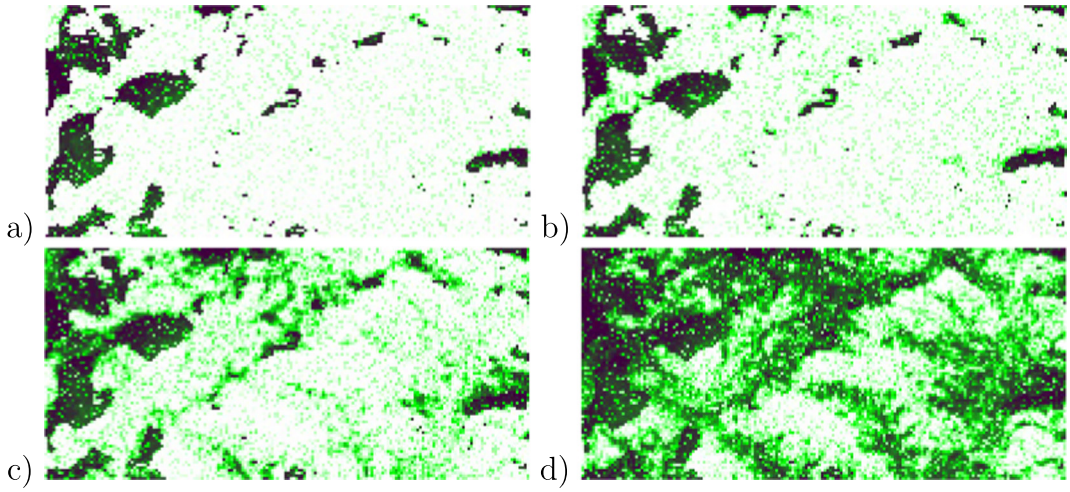


**Fig. 8.** Simulated tree cover distribution according to land-use scenarios (grazing pressure and single-tree cutting) in the computational domain of Fig. 2. The entire landscape was pastured except for several patches of forest, which are shown in dark green in panel a) and as dense and tall stands of trees in Figs. 4 and 5. Darker green tones indicate higher tree cover. a) Intensive grazing (0.9 ABU/ha for 124 days per year); b) maximum grazing (0.7 ABU/ha for 124 days per year); c) optimum grazing (0.5 ABU/ha for 124 days per year); d) minimum grazing (0.3 ABU/ha for 124 days per year). Grazing intensities are explained in the text.

minimized. While with the lowest grazing pressure (i.e. 0.3 ABU/ha) and consequently overall high tree cover, the WEP decrease is highest. This is consistent with the physics that the overall high surface roughness due to dense tree cover slows down the flow. The relative decrease of WEP can reach up to 40% in the case of poor pasture management and the development of a landscape mosaic where treeless grasslands decline and wooded habitats dominate (minimum grazing scenario). The loss of WEP is significant already with the dominance of sparsely-wooded habitats in the case of the optimum grazing scenario (0.7 ABU/ha). Forest development contributes less because in our case it is dominant in the valleys for which WEP is not evaluated. The importance of treeless grassland for WEP is shown by the optimum grazing scenario, where the prevail of sparsely-wooded habitats on the coast of grassland leads to a dramatic WEP decrease of 30%.

It is important to note that Fig. 10 demonstrates a non-linear relationship between WEP and overall tree cover. With only a slight increase of tree cover, WEP decreases rapidly when shifting from intensive (0.9 ABU/ha) to maximum grazing (0.7 ABU/ha). The reason is the emergence of scattered trees everywhere on the hilltops. They sum up to a relatively low tree cover but lead to high surface roughness. As a result, certain small changes in the landscape that may not be so obvious, can produce substantial decreases in WEP. These landscape changes may be significant already after 25 years of poor pasture-management or abandonment (Dovčiak et al., 2008) and dense thickets may even develop after 36 years (historical photographs of the area). Future climate warming will speed up tree growth in the mountains by prolonged growing seasons. The results generally support the argument that turbine installations should consider land management plans to ensure the expected energy production for their lifetime (typically around 20–25 years). This also implies that a single set of turbines can be in place for 25 years, then decommissioned, with new turbines installed in different locations. However, this has ramifications, like more roads and disturbance.

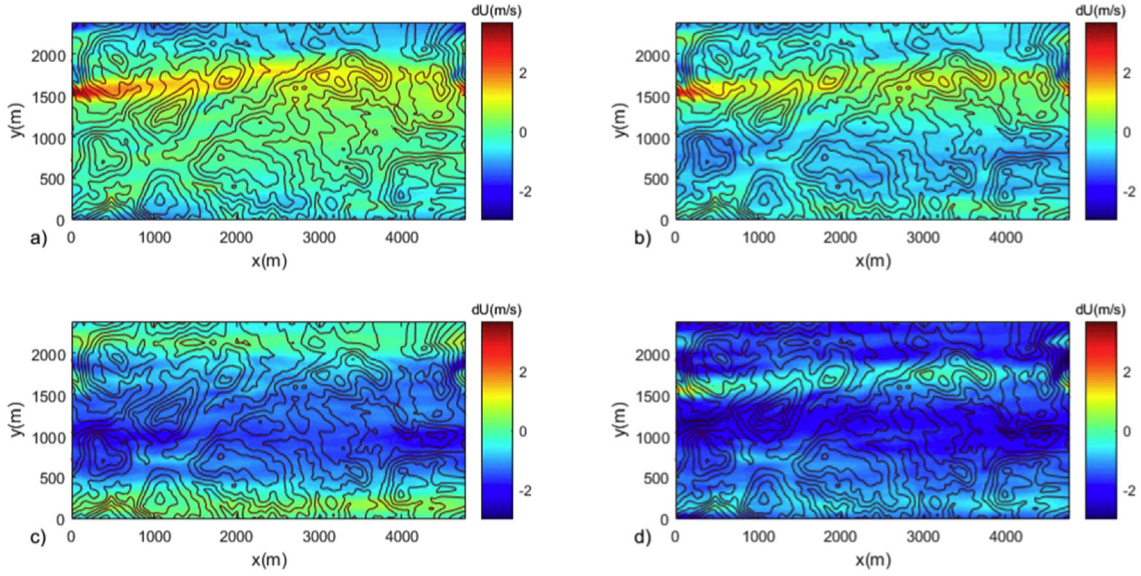


**Fig. 9.** The mean wind speed shift, respectively the difference with respect to the mean wind speed in the current landscape, for four different land-use scenarios: a) Intensive grazing; b) maximum grazing; c) optimum grazing; d) minimum grazing. Here the solid contour lines show the elevation.

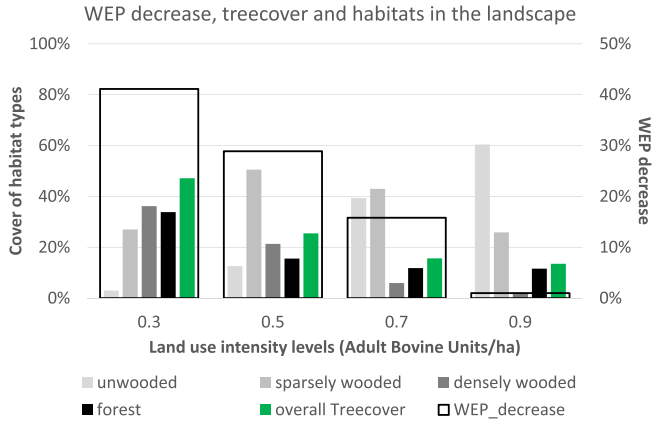


**Fig. 10.** The cover of habitat types and relative decrease of wind energy potential (WEP) for four different land-use scenarios: a) Intensive grazing (0.9 ABU/ha); b) maximum grazing (0.7 ABU/ha); c) optimum grazing (0.5 ABU/ha); d) minimum grazing (0.3 ABU/ha). Habitats are defined by tree cover classes. unwooded: 0–2%; sparsely wooded: 2–20%; densely wooded: 20–70%; forest: >70%.

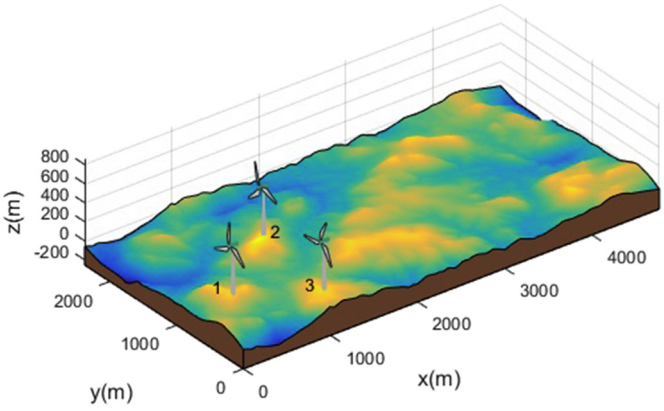


**Fig. 11.** Locations of the maximum mean wind speed for different land-use scenarios: 1) Present; 2) maximum grazing; 3) minimum grazing.

Moreover, Fig. 10 demonstrates a tradeoff between high WEP and structurally diverse landscapes with high habitat diversity and nature conservation value in combination with farmers' income. Intensive grazing cleans up the landscape from even scattered trees, providing low roughness and highest wind energy potential and highest agro-economic benefit, but densely wooded habitats lack. The recommended maximum grazing (0.7 ABU/ha) combines habitat provision for nature conservation purposes and high agro-economical incomes for local people. However, wind energy potential is suggested to be 15% lower. Optimal pasture management for a balanced habitat diversity (optimum grazing of 0.5 ABU/ha) is associated with a strong decrease of WEP and also lower income for farmers. The disregard of pasture-woodland maintenance (minimum grazing of 0.3 ABU/ha) not only leads to losses of biodiversity by the disappearance of treeless grassland habitats and to losses of local income but also dramatically decreases WEP. In summary, our simulations suggest that the potential to find a balance among WEP, agro-economic benefits to the local people and nature conservation interests lies in an optimized and integrated management scheme of the landscape and should be guaranteed by incentives from multiple sources. While agronomy departments may ensure human and nature aspects, wind energy companies are called to invest in proper land management that ensures constantly high energy yields.

Fig. 11 shows the locations of the maximum mean wind speed under the present land cover and two projected land covers due to land-use changes. It turns out that the location with the highest wind speed also changes from scenario to scenario. Therefore, when optimizing the micro-siting of wind turbines, the associated changes in the spatial distribution of mean wind speed must be taken into account to maximize wind energy production.

Fig. 12 shows the turbulence intensities (TI) at the surface of the turbine hub height for the four land-use scenarios. Interestingly, the spatial patterns of the TI distribution are similar between the various land-use scenarios, indicating that with respect to TI the terrain plays a dominant role as compared to the land cover. Nevertheless, the simulated landscape change for less than optimum pasture management (e.g. Fig. 12c) leads to larger areas to be affected by medium values of TI. This can be understood as an effect of the spread of scattered trees and the entire grassland-forest mosaic becoming more complex in pattern. Therefore, when optimizing the micro-siting of

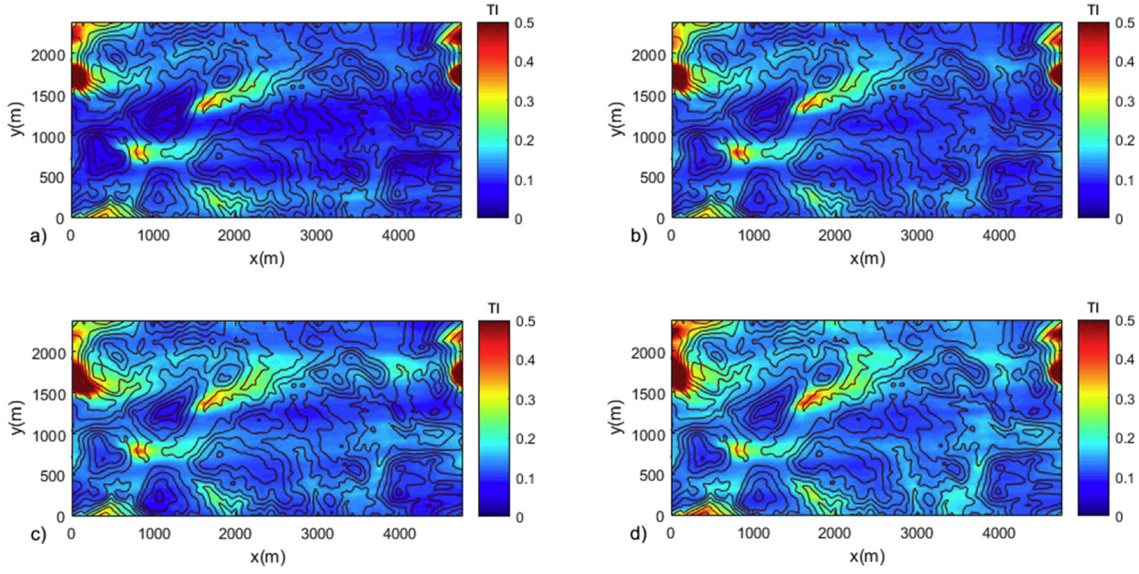


**Fig. 12.** Turbulence intensity distributions for four different land-use scenarios: a) Intensive grazing; b) maximum grazing; c) optimum grazing; d) minimum grazing. Here the solid contour lines show the elevation.

wind turbines, the changes in the spatial distribution of turbulence intensity associated with future landscape changes must be also taken into account to minimize turbine fatigue loads and associated maintenance costs.

## 4. Conclusions

The results of the case study demonstrate that the overall shifts in wind energy potential following the changes of vegetation pattern due to different land-use policies can be dramatic. This suggests that the wind power planning should be integrated with the land-use planning at a specific site to ensure that the expected energy production of the wind farm to be installed can be reached over its entire lifetime. Following a previously unexplored pathway of cause-effect relationships, a new linkage of agro- and forest policies to renewable energy production and biodiversity targets was demonstrated. Regarding the sustainable and optimized landscape management, there is a compromise to be targeted that balances biodiversity, agro-economic income and wind energy potential (WEP). Our coupled model also suggests non-linear relationships that may lead to strong decreases in WEP following only slight increase in tree cover. Moreover, the changes in the spatial distribution of wind and turbulence under different scenarios of land-use are complex. In particular, the location with the highest wind speed changes from scenario to scenario. Therefore, when optimizing the micro-siting of wind turbines, the associated changes in wind speed and turbulence must be taken into account to maximize wind energy production and minimize fatigue loads (and associated maintenance costs). The proposed new modeling framework offers, for the first time, a powerful tool for assessing vegetation dynamics induced long-term uncertainties in wind energy potential over complex terrain.

## Acknowledgments

This work was supported by the Swiss National Science Foundation in the framework of the Romanian-Swiss Research Programme, project WindLand, project codes: IZERZ0-142168 and 22 RO-CH/RSRP and was partially carried out within the frame of the Swiss Centre for Competence in Energy Research on the Future Swiss Electrical Infrastructure (SCCER-FURIES) with the financial support of the Swiss Innovation Agency (Innosuisse - SCCER program), contract number: 1155002544. Computing resources were provided by EPFL through the use of the facilities of its Scientific IT and Application Support Center and by the Swiss National Supercomputing Centre (CSCS). We wish to thank Magda Năpăruş-Aljančič for discussions regarding the GIS approaches and Ioana Stoicescu for fruitful collaboration in the field campaigns.

## Appendix A. WiRE-LES

LES is an eddy-resolving numerical model, which is superior to the conventional Reynolds-Averaged Navier-Stokes (RANS) approach in predicting unsteady turbulent flows. Computationally, LES is feasible for very high Reynolds number flows, such as the ABL, for which direct numerical simulation of the original N-S equations is unrealizable due to its requirement of using enough grid resolution to resolve turbulence from the energy-containing integral scale down to the Kolmogorov scale. In LES, turbulent eddies with scales larger than the grid scale are resolved and the net effect of the unresolved smaller scale motions is modeled by a subgrid-scale (SGS) model. The accuracy of LES relies on the SGS model. A major advancement in LES has been the introduction of the dynamic procedure (Germano et al., 1991), which eliminates the need of tuning parameters in SGS models. Based on the dynamic procedure, more advanced SGS models have been developed.

The WiRE-LES solves the three-dimensional spatially filtered N-S equations written in the rotational form as follows:

$$\frac{\partial \tilde{u}_i}{\partial x_i} = 0, \tag{A.1}$$

$$\frac{\partial \tilde{u}_i}{\partial t} + \tilde{u}_j\left(\frac{\partial \tilde{u}_i}{\partial x_j} - \frac{\partial \tilde{u}_j}{\partial x_i}\right) = -\frac{\partial \tilde{p}^*}{\partial x_i} + \nu\frac{\partial^2 \tilde{u}_i}{\partial x_j \partial x_j} - \frac{\partial \tau_{ij}}{\partial x_j} + F_i, \tag{A.2}$$

where $t$ denotes time, $\tilde{u}_i$ is the $i$-th component of the instantaneous resolved velocity, $x_i$ is the $i$-th component of the position vector, $\tilde{p}^* = \tilde{p}/\rho + \frac{1}{2}\tilde{u}_i\tilde{u}_i$ is the modified pressure with the density $\rho$ and resolved kinetic energy included, $\nu$ denotes the kinematic viscosity, and $\tau_{ij}$ is the $ij$-th component of the SGS stress tensor. Buoyancy effects are not considered in this study (i.e. neutral stability is assumed). The flow is driven by an external force **F**. Various SGS models are implemented in the WiRE-LES. Used in this study is the well-tested Lagrangian averaged scale-dependent dynamic model (Stoll and Porté-Agel, 2006) which is tuning-free and has been shown to be particularly well suited to capturing unresolved small-scale turbulence in complex environments (Stoll and Porté-Agel, 2006; Wan et al., 2007; Stoll and Porté-Agel, 2008; Cheng and Porté-Agel, 2013).

The incompressibility of the fluid expressed by Eq. (A.1) is satisfied by the projection method (Albertson and Parlange, 1999; Fang and Porté-Agel, 2016). All the involved partial differential equations are numerically solved by using a vertically-staggered grid arrangement with the spatial derivatives of flow variables in the horizontal and vertical directions being calculated based on the pseudo-spectral and second-order central difference methods respectively (Albertson and Parlange, 1999; Porté-Agel et al., 2000). This arrangement allows the Poisson's equation for pressure resulting from the projection method to be solved efficiently in each time step without the need of iteration when the terrain is flat. All non-linear terms are de-aliased in Fourier space by the 3/2 rule (Canuto et al., 1988). Time integration is done by the Adams-Bashforth scheme. High-performance computing techniques are utilized in the WiRE-LES to accelerate the calculations and make the computational cost of high-resolution simulation affordable. This is done through the parallelization using horizontal slab decomposition and MPI for inter-processor communication and the implementation of OpenMP within each MPI task.

In the simulation of turbulent flows over complex terrain (e.g., hills, mountains, urban areas), the complexity of topography leads to challenges in discretizing the computational domain. In the WiRE-LES, two methods of representing topography have been developed and implemented. They are the immersed boundary method (IBM) and the terrain-following coordinate transformation (TFCT) method (Wan et al., 2007; Cheng and Porté-Agel, 2013; Fang and Porté-Agel, 2016). The advantage of IBM is that no change has to be made for the conventional Cartesian grid. To model the topography effects on the flow, an artificial force is introduced to stop the flow inside the solid. In addition, proper interpolations for velocity near the solid surface are needed to satisfy the boundary conditions. Meanwhile, to enforce both no-slip and divergence-free conditions, the Poisson's equation for pressure should be solved together with the equation for the artificial force (Fang et al., 2011). In the terrain-following coordinate transformation method, the physical domain is discretized using a body-fitted grid. With the coordinate transformation defined as

$$\bar{x} = x, \quad \bar{y} = y, \quad \bar{z} = H\frac{z - z_s}{H - z_s}, \tag{A.3}$$

where $H$ is the maximum height of the domain and $z_s$ is the surface elevation, the grid becomes a regular one in the new coordinate system, so all calculations can be done using the same numerical schemes as for flat terrain. For the derivative calculations in the $x$, $y$,

$z$ frame, the chain rule is applied to derive the transform formulas. Accordingly, the Poisson's equation for pressure is rewritten for the new coordinate system and solved by an efficient iterative approach (Fang and Porté-Agel, 2016). The advantage of the TFCT method is that it facilitates the implementation of the wall boundary conditions since we have the grid points exactly on the wall. The disadvantage of TFCT is that it only works for topography with low to medium slope, while IBM is not subject to such a constraint.

When applying LES to solve turbulent flows over complex terrain at high Reynolds numbers, due to impractical refinement of the grid to resolve the small eddies in the roughness sublayer, the use of a wall model is a must. There exists currently no accurate wall model applicable for complex terrain. The WiRE-LES follows the common practice (Chester et al., 2007) to simply use the wall model based on MOST for flat walls. In the neutral case, the wall shear stress is calculated according to the logarithmic law for the velocity profile as

$$\tau_w = -\rho\left[\frac{\kappa\,|\mathbf{V}_t|}{\ln((z-d)/z_0)}\right]^2 \tag{A.4}$$

in a local coordinate system defined by the local tangential flow direction and the wall normal direction. In Eq. (A.4), $\kappa$ is the von Kármán constant, $z_0$ is the roughness length, $d$ is the displacement height, and $\boldsymbol{V}_t$ is the tangential velocity interpolated at a point with a normal distance $z$ to the solid surface. The stress is then transformed back to the original coordinate system.

## References


Albertson, J.D., Parlange, M.B., 1999. Surface length scales and shear stress: implications for land-atmosphere interaction over complex terrain. Water Resour. Res. 35 (7), 2121–2132.

Barbezat, V., Boquet, J.-F., 2008. Gestion intégrée des paysages sylvo-pastoraux de l'Arc jurassien - Manuel. Conférence TransJurassienne, La Chaux-de-Fonds.

Bechmann, A., Sørensen, N., 2011. Hybrid RANS/LES applied to complex terrain. Wind Energy 14 (2), 225–237.

Bergmeier, E., Petermann, J., Schröder, E., 2010. Geobotanical survey of wood-pasture habitats in Europe: diversity, threats and conservation. Biodivers. Conserv. 19, 2995–3014.

Bilal, M., Birkelund, Y., Homola, M., Virk, M., 2016. Wind over complex terrain - microscale modelling with two types of mesoscale winds at Nygårdsfjell. Renew. Energy 99, 647–653.

Buttler, A., Kohler, F., Gillet, F., 2009. The Swiss mountain wooded pastures: patterns and processes. In: Rigueiro-Rodriguez, A., McAdam, J., Mosquera-Losada, M. (Eds.), Agroforestry in Europe: Current Status and Future Prospects. Springer, New York, pp. 377–396.

Canuto, C., Hussaini, M., Quarteroni, A., Zang, T., 1988. Spectral Methods in Fluid Dynamics. Springer, New York.

Carvalho, D., Rocha, A., Santos, C., Pereira, R., 2013. Wind resource modelling in complex terrain using different mesoscale-microscale coupling techniques. Appl. Energy 108, 493–504.

Castro, F., Silva Santos, C., Lopes Da Costa, J., 2015. One-way mesoscale-microscale coupling for the simulation of atmospheric flows over complex terrain. Wind Energy 18 (7), 1251–1272.

Cheng, W.-C., Porté-Agel, F., 2013. Evaluation of subgrid-scale models in large-eddy simulation of flow past a two-dimensional block. Int. J. Heat Fluid Flow 44, 301–311.

Chester, S., Meneveau, C., Parlange, M.B., 2007. Modeling turbulent flow over fractal trees with renormalized numerical simulation. J. Comput. Phys. 225 (1), 427–448.

Diebold, M., Higgins, C., Fang, J., Bechmann, A., Parlange, M.B., 2013. Flow over hills: a large-eddy simulation of the bolund case. Bound.-Layer Meteorol. 148 (1), 177–194.

Dovčiak, M., Hrivnák, R., Ujházy, K., Gömöry, D., 2008. Seed rain and environmental controls on invasion of *Picea abies* into grassland. Plant Ecol. 194 (1), 135–148.

Dragomir, G., Şerban, A., Năstase, G., Brezeanu, A., 2016. Wind energy in Romania: a review from 2009 to 2016. Renew. Sustain. Energy Rev. 64, 129–143.

Dufour, A., Gadallah, Z., Wagner, H., Guisan, A., Buttler, A., 2006. Plant species richness and environmental heterogeneity in a mountain landscape: effects of variability and spatial configuration. Ecography 29, 573–584.

Etienne, M., 1996. Western European Silvopastoral Systems. INRA, Paris.

Fang, J., Diebold, M., Higgins, C., Parlange, M.B., 2011. Towards oscillation-free implementation of the immersed boundary method with spectral-like methods. J. Comput. Phys. 230 (22), 8179–8191.

Fang, J., Porté-Agel, F., 2016. Intercomparison of terrain-following coordinate transformation and immersed boundary methods in large-eddy simulation of wind fields over complex terrain. J. Phys. Conf. Ser. 753 (8), 082008.

Gallandat, J.-D., Gillet, F., Havlicek, E., Perrenoud, A., 1995. Typologie et systémique phyto-écologiques des pâturages boisés du Jura suisse. Tech. Rep. rapport final de mandat Offices fédéraux et cantonaux, Laboratoire d'écologie végétale, Université de Neuchâtel, Neuchâtel, Switzerland.

Germano, M., Piomelli, U., Moin, P., Cabot, W., 1991. A dynamic subgrid-scale eddy viscosity model. Phys. Fluids A 3 (7), 1760–1765.

Gillet, F., 2008. Modelling vegetation dynamics in heterogeneous pasture-woodland landscapes. Ecol. Model. 217, 1–18.

Gillet, F., Murisier, B., Buttler, A., Gallandat, J.-D., Gobat, J.M., 1999. Influence of tree cover on diversity of herbaceous communities in subalpine wooded pastures. Appl. Veg. Sci. 2, 47–54.

Gopalan, H., Gundling, C., Brown, K., Roget, B., Sitaraman, J., Mirocha, J., Miller, W., 2014. A coupled mesoscale-microscale framework for wind resource estimation and farm aerodynamics. J. Wind Eng. Ind. Aerodyn. 132, 13–26.

Hahmann, A., Vincent, C., Peña, A., Lange, J., Hasager, C., 2015. Wind climate estimation using WRF model output: method and model sensitivities over the sea. Int. J. Climatol. 35 (12), 3422–3439.

Jiménez, P., Dudhia, J., 2012. Improving the representation of resolved and unresolved topographic effects on surface wind in the WRF model. J. Appl. Meteorol. Climatol. 51 (2), 300–316.

Jiménez, P., Dudhia, J., 2013. On the ability of the WRF model to reproduce the surface wind direction over complex terrain. J. Appl. Meteorol. Climatol. 52 (7), 16101617.

Liu, Z., Ishihara, T., Tanaka, T., He, X., 2016. LES study of turbulent flow fields over a smooth 3-d hill and a smooth 2-d ridge. J. Wind Eng. Ind. Aerodyn. 153, 1–12.

Lu, H., Porté-Agel, F., 2011. Large-eddy simulation of a very large wind farm in a stable atmospheric boundary layer. Phys. Fluids 23 (6), 065101.

Maruska, T., Mocanu, V., Blaj, V., 2012. Agrosilvopastoral system and food security in the context of global warming. Annals of the Academy of Romanian Scientists, Series on Agriculture Forestry and Veterinary Medicine Sciences 1, 131–140.

Mirocha, J., Kosović, B., Kirkil, G., 2014. Resolved turbulence characteristics in large-eddy simulations nested within mesoscale simulations using the weather research and forecasting model. Mon. Weather Rev. 142 (2), 806–831.

Moeng, C.-H., Dudhia, J., Klemp, J., Sullivan, P., 2007. Examining two-way grid nesting for large eddy simulation of the PBL using the WRF model. Mon. Weather Rev. 135 (6), 2295–2311.

Munteanu, C., Kuemmerle, T., Boltiziar, M., Butsic, V., Gimmi, U., Halada, L., Kaim, D., Király, G., Konkoly-Gyuró, E., Kozak, J., Lieskovský, J., Mojses, M., Müller, D., Ostafin, K., Ostapowicz, K., Shandra, O., Štych, P., Walker, S., Radeloff, V., 2014. Forest and agricultural land change in the Carpathian region – a meta-analysis of long-term patterns and drivers of change. Land Use Policy 38, 685–697.

Nolan, P., Lynch, P., Sweeney, C., 2014. Simulating the future wind energy resource of Ireland using the COSMO-CLM model. Wind Energy 17 (1), 19–37.

Peringer, A., Rosenthal, G., 2011. Establishment patterns in a secondary tree line ecotone. Ecological Modelling 222 (17), 3120–3131. https://doi.org/10.1016/j.ecolmodel.2011.05.025.

Peringer, A., Schulze, K., Stupariu, I., Stupariu, M., Rosenthal, G., Buttler, A., Gillet, F., 2016. Multi-scale feedbacks between tree regeneration traits and herbivore behavior explain the structure of pasture-woodland mosaics. Landsc. Ecol. 31 (4), 913–927.

Peringer, A., Siehoff, S., Chételat, J., Spiegelberger, T., Buttler, A., Gillet, F., 2013. Past and future landscape dynamics in pasture-woodlands of the Swiss Jura Mountains under climate change. Ecol. Soc. 18 (3), 11.

Perrenoud, A., Känzig-Schoch, U., Schneider, O., Wettstein, J.B., 2003. Exploitation durable des pâturages boisés. Un exemple appliqué de Jura suisse. Haupt Verlag, Bern.

Porté-Agel, F., Meneveau, C., Parlange, M.B., 2000. A scale-dependent dynamic model for large-eddy simulation: application to a neutral atmospheric boundary layer. J. Fluid Mech. 415, 261–284.

Pătru-Stupariu, I., Stupariu, M., Stoicescu, I., Peringer, A., Buttler, A., Fürst, C., 2017. Integrating geo-biodiversity features in the analysis of landscape patterns. Ecol. Indic. 80, 363–375.

Pătru-Stupariu, I., Tudor, A., Stupariu, M., Buttler, A., Peringer, A., 2016. Landscape persistence and stakeholder perspectives: the case of Romania's Carpathians. Appl. Geogr. 69, 87–98.

Raupach, M.R., 1994. Simplified expressions for vegetation roughness length and zero–plane displacement as functions of canopy height and area index. Bound.-Layer Meteorol. 71, 211–216.

Sanz Rodrigo, J., Chávez Arroyo, R., Moriarty, P., Churchfield, M., Kosović, B., Réthoré, P.-E., Hansen, K., Hahmann, A., Mirocha, J., Rife, D., 2017. Mesoscale to microscale wind farm flow modeling and evaluation. Wiley Interdisciplinary Reviews: Energy and Environment 6 (2), e214.

Shamsoddin, S., Porté-Agel, F., 2017. Large-eddy simulation of atmospheric boundary-layer flow through a wind farm sited on topography. Bound.-Layer Meteorol. 163 (1), 1–17.

Silva Lopes, A., Palma, J., Castro, F., 2007. Simulation of the Askervein flow. Part 2: large-eddy simulations. Bound.-Layer Meteorol. 125 (1), 85–108.

Skamarock, W.C., Klemp, J.B., Dudhia, J., Gill, D.O., Barker, D.M., Duda, M.G., Huang, X.-Y., Wang, W., Powers, J.G., 2008. A description of the advanced research WRF version 3. Tech. Rep. NCAR/TN-475+STR, National Center for Atmospheric Research, Boulder, Colorado, USA. June.

Stoll, R., Porté-Agel, F., 2006. Dynamic subgrid-scale models for momentum and scalar fluxes in large-eddy simulations of neutrally stratified atmospheric boundary layers over heterogeneous terrain. Water Resour. Res. 42 (1), W01409.
Stoll, R., Porté-Agel, F., 2008. Large-eddy simulation of the stable atmospheric boundary layer using dynamic models with different averaging schemes. Bound.-Layer Meteorol. 126 (1), 1–28.
Wan, F., Porté-Agel, F., 2010. Large-eddy simulation of stably-stratified flow over a steep hill. Bound.-Layer Meteorol. 138 (3), 367–384.
Wan, F., Porté-Agel, F., 2011. A large-eddy simulation study of turbulent flow over multiscale topography. Bound.-Layer Meteorol. 141 (2), 201–217.
Wan, F., Porté-Agel, F., Stoll, R., 2007. Evaluation of dynamic subgrid-scale models in large-eddy simulations of neutral turbulent flow over a two-dimensional sinusoidal hill. Atmos. Environ. 41 (13), 2719–2728.
Weisberg, P.J., Coughenour, M.B., Bugmann, H., 2006. Modelling of large herbivore-vegetation interactions. In: Danell, K., Bergström, R., Duncan, P., Pastor, J. (Eds.), Large Herbivore Ecology, Ecosystem Dynamics and Conservation. Cambridge Univ. Press, Cambridge, pp. 348–382.
Wood, N., 2000. Wind flow over complex terrain: a historical perspective and the prospect for large-eddy modelling. Bound.-Layer Meteorol. 96 (1–2), 11–32.
Wu, Y.T., Porté-Agel, F., 2011. Large-eddy simulation of wind-turbine wakes: evaluation of turbine parametrisations. Bound.-Layer Meteorol. 138 (3), 345–366.